Quasifree $(e, e'p)$ reactions on nuclei with neutron excess

C. Giusti, A. Meucci, F. D. Pacati
Dipartimento di Fisica Nucleare e Teorica, Università di Pavia, Pavia, ITALY
INFN, Sezione di Pavia, Via Bassi 6, I-27100 Pavia, ITALY

G. Co', V. De Donno
Dipartimento di Fisica, Università del Salento, Lecce, ITALY
INFN, Sezione di Lecce, Via Arnesano, I-73100 Lecce, ITALY

(Dated: August 31, 2011)

We study the evolution of the $(e, e'p)$ cross section on nuclei with increasing asymmetry between the number of neutrons and protons. The calculations are done within the framework of the distorted-wave impulse approximation, by adopting nonrelativistic and relativistic models. We compare the results obtained with three different approaches based on the mean-field description for the proton bound state wave function. In the nonrelativistic model phenomenological Woods-Saxon and Hartree-Fock wave functions are used, in the relativistic model the wave functions are solutions of Dirac-Hartree equations. The models are first tested against experimental data on ^{16}O, ^{40}Ca, and ^{48}Ca nuclei, and then they are applied to calculate $(e, e'p)$ cross sections for a set of spherical calcium and oxygen isotopes. From the comparison of the results obtained for the various isotopes we can infer information about the dependence of the various ingredients of the models on the neutron to proton asymmetry.

PACS numbers: 25.30.Fj; 21.60.Jz; 24.10.Jv

I. INTRODUCTION

The understanding of the evolution of the nuclear properties with respect to the asymmetry between the number of neutrons and protons is one of the major topics of interest in modern nuclear physics. It is going to extend our knowledge about the effects of isospin asymmetry on the nuclear structure, and is also relevant for the study of the origin and the limits of stability of matter in the universe.

Nuclear reactions represent our main source of information on the properties and on the structure of atomic nuclei. Direct nuclear reactions, where the external probe interacts with only one, or a few, nucleons of the target nucleus, can give deep insight on the single-particle (s.p.) properties of a many-body system. In particular, the $(e, e'p)$ reaction, where a proton is emitted with a direct knockout mechanism, represents a very clean probe to explore thestructure pf the proton-hole states of the nucleus [1–3].

Electron scattering is probably the best tool for investigating the structure of atomic nuclei and their constituents. The electromagnetic interaction is weak if compared with the strength of the interaction between hadrons, therefore the nuclear many-body system is only slightly perturbed by the probe. In addition, the possibility of varying independently the energy and momentum transferred to the nucleus allows us to map the nuclear response as a function of the excitation energy with a space resolution that can be adjusted to the scale of processes we want to study. The theoretical description of the electron-nucleus interaction is well controlled by the perturbative quantum electrodynamics theory, and, for the energies used in nuclear physics investigations, the one-photon exchange approximation is usually enough to obtain a good description of the electron scattering process. The advantages of electron scattering have been exploited in the past to study the properties of stable nuclei. These studies can now be extended to exotic nuclear matter.

In the last thirty years a large amount of $(e, e'p)$ data has provided accurate informations on the s.p. structure of stable closed-shell nuclei. Many high-resolution exclusive $(e, e'p)$ experiments on several stable nuclei were carried out at Saclay [1–5], NIKHEF [2, 3, 6, 7] and MAMI [8]. Specific quantum numbers and spectroscopic factors have been assigned to the peaks in the energy spectrum by studying the missing energy and momentum dependence of the experimental cross sections. The data analysis was carried out by using the program `DWEEPY` [9, 10] which describes the process within the theoretical framework of the nonrelativistic distorted-wave impulse approximation

(DWIA). In the program the effects of the final-state interactions (FSI) due to the reinteraction of the emitted proton with the remaining nucleus and also the distortion of the electron wave functions produced by the nuclear Coulomb field are included. For the data analysis, phenomenological ingredients were usually adopted to calculate the s.p. bound and scattering states. In the original analyses of the experimental data, the outgoing nucleon scattering wave functions were eigenfunctions of an optical potential determined through a fit to elastic unpolarized and polarized nucleon-nucleus scattering data.

The bound-state wave functions were calculated with a Woods-Saxon (WS) well, where the radius was determined to fit the experimental momentum distribution and the depth was adjusted to give the experimentally observed separation energy of the bound final state. This theoretical approach was able to describe, with a high degree of accuracy, for a wide range of nuclei and for different kinematics, the shape of the experimental momentum distributions at missing-energy values corresponding to specific peaks in the energy spectrum. In order to reproduce the size of the experimental cross sections, the normalization of the bound-state wave function was fitted to the data and identified with the spectroscopic factor. The deviations of such normalization factors from the predictions of the mean-field (MF) approximation are interpreted as the effect of nucleon-nucleon correlations.

The description of $(e, e'p)$ processes was done also with relativistic DWIA (RDWIA) models [11–28]. In these approaches the s.p. bound-state wave functions are obtained by solving Dirac-Hartree equations with an interaction obtained by a relativistic Lagrangian written in the context of the relativistic MF theory. The scattering wave functions are obtained by solving the Dirac equation with relativistic optical potentials determined by a fit to elastic proton-nucleus scattering data. Some of these models include also an exact treatment of the Coulomb distortion of the electron waves [12, 13, 15–17]. The RDWIA calculations, which provide a good description of the old $(e, e'p)$ data, are necessary for the analysis of the more recent $(e, e'p)$ data from JLab [29, 30], measured in kinematic conditions with higher values of the momentum transfer and of the outgoing proton energy, unachievable in previous experiments.

In upcoming years the advent of radioactive ion beams facilities [31–33] will provide a large amount of data on unstable nuclei. A new generation of electron colliders that use storage rings is under construction at RIKEN (Japan) [34, 35] and GSI (Germany) [36]. These facilities will offer unprecedented opportunities to study the structure of exotic unstable nuclei through electron scattering in the ELISe experiment at FAIR in Germany [37] and the SCRIT project in Japan [38].

Kinematically complete experiments, where all target-like reaction products are detected, will become feasible for the first time, allowing a clean separation of different reaction channels as well as a reduction of the unavoidable radiative background seen in conventional experiments. Therefore, even applications to stable isotope will be of interest.

In this work we investigate how the models successfully used to describe $(e, e'p)$ data in stable nuclei behave when they are used to make predictions on exotic nuclei. In our study, we consider both the nonrelativistic (DWIA) and the relativistic (RDWIA) approaches, and we apply them to a set of calcium and oxygen isotopes. We have chosen these isotopes since data taken at NIKHEF for the doubly magic nuclei ^{40}Ca, ^{48}Ca [39, 40], and ^{16}O [41] are available. We first compare the performances of our models in describing these data, then we apply them to some even-even isotopes of these nuclei. We apply our models to ^{40,48,52,60}Ca and ^{16,22,24,28}O nuclei, where the s.p. levels below the Fermi surface are fully occupied. In this manner we work with spherical systems and minimize the pairing effects. Our models require the description of both ground and excited states of the nuclear system, the latter one has a particle in the continuum. In this article, we investigate how different descriptions, apparently equivalent for stable nuclei, can produce different results when applied to neutron rich nuclei. The DWIA calculations are carried out with the same code `DWEEPY` that was used for the analyses of the experimental data. In the comparison with data we repeat the original analyses and present the results of calculations performed under the same conditions as in Refs. [39–41]. The results obtained with phenomenological WS wave functions are compared with those obtained by solving Hartree-Fock (HF) equations with Gogny-like finite-range interactions. The RDWIA calculations are performed with the fully relativistic model developed in Ref. [23]. The theoretical investigation of exotic nuclei with models of proven reliability in stable isotopes will test the ability of the established nuclear theory in the domain of exotic nuclei, revealing the evolution of nuclear properties as a function of the asymmetry between the number of neutrons and protons. Moreover, it will provide valuable references for future experiments.

The paper is organized as follows. In Sec. II, we outline the basic aspects of the models used for the calculations. We present and discuss our results in Sec. III and we draw our conclusions in Sec. IV.

II. THEORETICAL DESCRIPTION OF THE $(e, e'p)$ PROCESS

Our description of the $(e, e'p)$ reactions is based on the one-photon exchange approximation, where the incident electron exchanges a virtual photon, of momentum $\boldsymbol{q}$ and energy ω, with the target nucleus [3]. In this approximation,

the evaluation of the cross section requires the calculation of the contraction between the lepton tensor, that contains the electron current, and the hadron tensor, that contains the nuclear electromagnetic current. If we neglect the effects of the nuclear Coulomb field on the electrons, the initial and final electron wave functions are plane wave solutions of the Dirac equation. In this case, we can write the lepton tensor as a kinematical factor, and the hadron tensor as a bilinear product of the Fourier transforms of the transition matrix elements of the nuclear electromagnetic current operator between the initial $|\Psi_{\rm i}\rangle$ and final $|\Psi_{\rm f}\rangle$ nuclear states

$$J^\mu(\boldsymbol{q}) = \int \langle \Psi_{\rm f}|\hat{J}^\mu(\boldsymbol{r})|\Psi_{\rm i}\rangle \, {\rm e}^{\,{\rm i}\boldsymbol{q}\cdot\boldsymbol{r}} d^3r \ . \tag{1}$$

If Coulomb-distorted electron wave functions are considered in the model, the transition matrix element of the electron current replaces the exponential in Eq. (1) and the calculation becomes much more complicated [3, 9, 10, 15]. For the nuclei and the electron energies considered in this work, however, a simple and accurate enough method to include the effects of Coulomb distortion is to preserve the expression (1) but using an effective momentum transfer and change the momentum transfer into an effective momentum transfer [3, 9, 10, 15]. Therefore in all the calculations presented in this paper we have used this approximation.

The evaluation of the expression (1) requires a model that describes the initial and final nuclear many-body states. A detailed description of our DWIA model, and of the related assumptions, can be found in Refs. [3, 42]. In short, we assume that in the final state the residual nucleus, that is composed by $A-1$ nucleons, is left in a bound state $|\Psi^{\rm B}_\alpha(E)\rangle$, characterized by the energy E and the quantum numbers α. Then, for the final nuclear state we select the channel subspace spanned by the wave function $|\Psi^{\rm B}_\alpha(E)\rangle$, describing the $A-1$ nucleons, and a function describing the state of the emitted nucleon. Moreover, we assume the direct knockout mechanism, where the one-body nuclear electromagnetic current operator acts exclusively on the space spanned by this type of many-body states.

Under these assumptions we can write the expression (1) as

$$\begin{aligned} J^\mu(\boldsymbol{q}) &= \int \langle \Psi_{\rm f}|a^\dagger(\boldsymbol{r})|\Psi^{\rm B}_\alpha(E)\rangle \, \hat{\jmath}^\mu(\boldsymbol{r}) \, \langle \Psi^{\rm B}_\alpha(E)|a(\boldsymbol{r})|\Psi_{\rm i}\rangle \, {\rm e}^{\,{\rm i}\boldsymbol{q}\cdot\boldsymbol{r}} \, d^3r \\ &= \int \chi^{(-)*}_{E\alpha}(\boldsymbol{r}) \, \hat{\jmath}^\mu(\boldsymbol{r}) \, \phi_{E\alpha}(\boldsymbol{r}) \, [S_\alpha(E)]^{1/2} \, {\rm e}^{\,{\rm i}\boldsymbol{q}\cdot\boldsymbol{r}} \, d^3r \ , \end{aligned} \tag{2}$$

where we have not explicitly indicated the dependence on the spin and isospin variables and we understand that the one-body electromagnetic current operator $\hat{\jmath}^\mu$ acts on the nuclear wave fuctions only. In Eq. (2) we have indicated with $a(\boldsymbol{r})$ the operator which annihilates a nucleon with coordinate $\boldsymbol{r}$, and with $\chi^{(-)}_{E\alpha}$ the distorted wave function of the emitted nucleon

$$\langle \Psi^{\rm B}_\alpha(E)|a(\boldsymbol{r})|\Psi_{\rm f}\rangle = \chi^{(-)}_{E\alpha}(\boldsymbol{r}) \ . \tag{3}$$

In the initial state for the wave function of the bound nucleon we have defined the overlap function, which describes the residual nucleus as a hole state in the target, as

$$\langle \Psi^{\rm B}_\alpha(E)|a(\boldsymbol{r})|\Psi_{\rm i}\rangle = [S_\alpha(E)]^{1/2} \, \phi_{E\alpha}(\boldsymbol{r}) \ . \tag{4}$$

The overlap function contains the effects of nuclear correlations [3, 43–45]. In the definition Eq. (4) the function $\phi_{E\alpha}(\boldsymbol{r})$ is normalized to unity. The spectroscopic factor $S_\alpha(E)$ is the norm of the overlap function and gives the probability of removing from the target a nucleon at $\boldsymbol{r}$ leaving the residual nucleus in the state $\Psi^{\rm B}_\alpha(E)$.

This model can be formulated in both the DWIA and the RDWIA. In RDWIA calculations four-vector relativistic wave functions for the initial bound and the final scattering states and, coherently, relativistic expressions for the nuclear current operator are used [23]. We point out that in our DWIA calculations some relativistic corrections are included in the kinematics and in the nuclear current operator.

Formally, as described in Refs. [3, 42], the s.p. scattering and bound state wave functions are derived in the model of Eq. (2) as eigenfunctions of an energy-dependent non-Hermitean Feshbach-type optical-model Hamiltonian. Such a consistent treatment is extremely difficult and, at present, bound and scattering states calculated from the theoretical optical potential are not available. For this reason, in actual calculations phenomenological wave functions are usually employed. In the nonrelativistic DWIA calculations, the outgoing proton wave functions are eigenfunctions of the complex phenomenological energy-dependent and A-dependent optical potential of Ref. [46], that contains a central and a spin-orbit term, and also a term dependent on the nuclear asymmetry $(N-Z)/A$. This is the same optical potential used in the original analyses of the NIKHEF data [39–41]. We used this potential in all the DWIA calculations done for the various isotopes we have investigated.

In our RDWIA model, the ejectile wave function is written in terms of its positive energy component Ψ_{f+} following the direct Pauli reduction method [47]. This scheme appears simpler and it is equivalent to the solution of the

Dirac equation. The resulting Schrödinger-like equation for Ψ_{f+} contains equivalent nonrelativistic central and spin-orbit potentials which are functions of the relativistic, energy-dependent, scalar and vector potentials. The Darwin nonlocality factor, that contains the effect of the negative-energy components of the spinor, is reabsorbed in the current operator, which becomes an effective relativistic one-body operator depending on the Dirac scalar and vector potentials as well as on the prescription for the electromagnetic current.

In our calculations we used the relativistic EDAD1 potential of Ref. [48], constructed to fit proton elastic scattering data on several nuclei in an energy range up to 1040 MeV.

The s.p. bound-state wave functions $\phi_{E\alpha}$ have been obtained in a MF model, and the values of the spectroscopic factors have been set to unity. In this article we intend to study the sensitivity of our results to the changes of the hole s.p. wave function. To this aim, we have performed calculations for the various nuclei under investigation with different MF approaches.

In a first approach, for the DWIA calculations, we repeat for the comparison with data the original analyses of Refs. [39–41] and adopt the same phenomenological ingredients. As indicated in the introduction, in these calculations the hole wave functions are calculated by using a WS well where the values of the depth and of the radius are adjusted to reproduce, respectively, the experimentally observed separation energy of the bound final state and the width of the experimental momentum distributions. The values of the parameters used in the calculations can be found in Refs. [39–41]. In order to reproduce the magnitude of the experimental cross sections a multiplicative reduction factor is applied to the calculated cross sections. These factors, identified with the spectroscopic factors, indicate that in $(e, e'p)$ reactions the removal of the MF s.p. strength for quasi-hole states near the Fermi energy is about 60-70% of the prediction of the s.p. model [3, 7, 40]. This information from $(e, e'p)$ experiments is up to now limited to stable isotopes.

The source of the reduction of the $(e, e'p)$ spectroscopic factor with respect to the MF value has been investigated by using various methodologies which consider different types of correlations, i. e., effects beyond the MF model. The short-range and tensor correlations, which arise from the characteristics of the bare nucleon-nucleon interaction, account for a reduction factor of at most 10-15% [49–54]. The remaining, and larger, part of the quenching is due to long-range correlations related to the coupling between s.p. motion and collective surface vibrations [45, 55].

In a second approach, also used in DWIA calculations, the hole s.p. wave functions are obtained by solving HF equations with the technique presented in Refs. [56, 57]. In these calculations we use two different parameterizations of the finite-range Gogny interactions, the more traditional D1S force [58] and the new D1M force [59]. The differences between the results obtained with these two forces are rather small when compared with the differences with the results obtained with the other methods. For this reason we shall present here only the results obtained with the D1M interaction, which produces a neutron matter equation of state which has a plausible behavior at high densities, in contrast to that obtained with the D1S interaction.

In the third approach we made RDWIA calculations where the hole wave functions are obtained in the context of the relativistic MF approach by solving the Dirac-Hartree equations. The nucleon interaction is derived from a relativistic Lagrangian containing σ, ω and ρ meson fields and also the photon field. The nuclear and Coulomb potentials are obtained by solving self-consistently the Klein-Gordon and Maxwell equations. This approach satisfactorily reproduces global and s.p. properties of several nuclei [60–62].

The last ingredient necessary to calculate the expression (2) is the current $\hat{j}^\mu$. In RDWIA calculations the electromagnetic one-body current operator corresponds to the relativistic current-conserving $cc2$ expression of Ref. [63]. This expression is consistent with the current we use in DWIA calculations, where the relativistic corrections up to order $1/M^2$, where M is the nucleon mass, are obtained from a Foldy-Wouthuysen transformation applied to the interaction Hamiltonian where the nuclear current has the same form as in the $cc2$ expression.

The values of some quantities related to the wave functions and density distributions, obtained in the different MF approaches for the nuclei under investigation, are compared in Tab. I for the oxygen isotopes and in Tab. II for the calcium isotopes. In these tables the proton separation energies and the root mean squared (rms) radii of the bound state wave functions are shown. The proton separation energies of the WS calculations reproduce the experimental values. For ^{28}O and ^{60}Ca nuclei, where no experimental values are available, the depth of the WS well has been chosen to reproduce the separation energy obtained in the nonrelativistic HF approach. We remark that, experimentally, ^{28}O and ^{60}Ca nuclei are unbound; however our MF calculations bind all the nuclei we have investigated.

In Tab. I and II we also present the rms radii of the global proton and neutron density distributions for the HF and the relativistic models. In the phenomenological WS approach the parameters of the WS well are determined to reproduce the experimental separation energy and the width of the experimental $(e, e'p)$ distribution and can give information only on the wave function of the considered proton. The behavior of the neutron rms radii is rather obvious and increases with the increasing number of neutrons. In the HF model the neutron radii are slightly smaller than in the relativistic model, but for ^{16}O and ^{40}Ca, where they are practically the same. The behavior of the proton rms radii is less obvious. The proton number is the same in each isotope chain, but in the HF case we observe a small increase of the proton rms radius with the increasing number of neutrons. In contrast, in the relativistic case there is

a slight decrease of the radius from ^{16}O to ^{22}O and from ^{40}Ca to ^{48}Ca, then for nuclei with larger neutron excess the radius increases. In general in the HF approach the proton radii are a bit larger than in the relativistic approach.

The modifications of the proton radii due to the presence of neutrons are related to the proton-neutron interaction, which is responsible also for the value of the proton-neutron symmetry energy in nuclear matter. In HF calculation we obtain a value of 29.45 MeV while that of the relativistic calculation is 35 MeV. These values should be compared with an empirical value of 32±3 MeV.

The experimental data of the $(e, e'p)$ reaction are separated in different peaks corresponding to specific values of the missing energy $E_{\rm m} = \omega - T' - T_{\rm B} = S_{\rm p} + E_{\rm x}$, where T' and $T_{\rm B}$ are the kinetic energies of the outgoing nucleon and of the residual nucleus, respectively, $S_{\rm p}$ is the nucleon separation energy, and $E_{\rm x}$ is the excitation energy of the residual nucleus. For each peak, the data are usually presented in terms of the reduced cross section as a function of the missing momentum $p_m = |\boldsymbol{p}_{\rm m}|$, which is the magnitude of the recoil momentum of the residual nucleus [3, 6, 7]. The reduced cross section is the cross section divided by a kinematical factor and by the elementary off-shell electron-proton scattering cross section. For the latter cross section, the $cc1$ prescription of Ref. [63] is usually adopted. In the reduced cross section the complicated dependence of the cross section on the kinematic variables is reduced to a twofold function of $E_{\rm m}$ and $p_{\rm m}$.

If we neglect FSI the wave function of the emitted proton is a plane wave. In this plane-wave impulse approximation (PWIA), the missing momentum $\boldsymbol{p}_{\rm m}$ corresponds, apart for a minus sign, to the initial momentum of the emitted nucleon in the nucleus. In the PWIA the cross section is factorized into the product of a kinematical factor, the elementary off-shell electron-proton scattering cross section, and the hole spectral function. Thus, in the PWIA the reduced cross section is the squared Fourier transform of the hole wave function, and can be interpreted as the momentum distribution of the emitted proton when it was inside the nucleus. This factorization is destroyed in the DWIA by FSI. However, even in the DWIA, the reduced cross section is an interesting quantity that can be regarded as the nucleon momentum distribution modified by FSI.

The theoretical approaches outlined above have been used to calculate $(e, e'p)$ reduced cross sections in the parallel and perpendicular kinematics selected in the experiments. In the so-called parallel kinematics [3], the momentum of the outgoing proton $\boldsymbol{p}'$ is kept fixed and taken parallel, or antiparallel, to the direction of the momentum transfer $\boldsymbol{q}$. Different values of the missing momentum $p_{\rm m}$ are obtained by varying the electron scattering angle and, as a consequence, q. In the so-called perpendicular, or $(\boldsymbol{q}, \omega)$ constant kinematics, the momentum transfer $\boldsymbol{q}$ and the outgoing proton momentum $\boldsymbol{p}'$ are kept constant and the value of the missing momentum $p_{\rm m}$ is changed by varying the angle of the outgoing proton.

III. RESULTS

In this section we present the results of our calculations of the exclusive $(e, e'p)$ cross sections for a set of oxygen and calcium isotopes. We compare the results obtained by using the different nuclear structure models described in the previous section. First we show the performances of the various models in the description of the existing experimental data in ^{40}Ca, ^{48}Ca, and ^{16}O nuclei. Then we present the results obtained for the other isotopes.

Measurements for the ^{40}Ca $(e, e'p)$ reaction were carried out at NIKHEF in both parallel and $(\boldsymbol{q}, \omega)$ constant kinematics [39]. The comparison with the experimental reduced cross sections in both kinematics is displayed in Fig. 1. We have considered the transitions to the $3/2^+$ ground state of the ^{39}K nucleus, corresponding to the knockout of the proton from the $1d_{3/2}$ s.p. level, and to the $1/2^+$ excited state of the ^{39}K nucleus at $E_{\rm x} = 2.522$ MeV, obtained by knocking out a proton from the $2s_{1/2}$ s.p. level. In Fig. 1, as well as in the subsequent figures, positive (negative) values of $p_{\rm m}$ refer to situations where in $(\boldsymbol{q}, \omega)$ constant kinematics the angle between the outgoing proton momentum $\boldsymbol{p}'$ and the incident electron $\boldsymbol{p}_0$ is larger (smaller) than the angle between $\boldsymbol{q}$ and $\boldsymbol{p}_0$. In parallel kinematics positive and negative values of $p_{\rm m}$ indicate, respectively, the $|\boldsymbol{q}| < |\boldsymbol{p}'|$ and $|\boldsymbol{q}| > |\boldsymbol{p}'|$ cases.

All the theoretical results shown in the figure provide a good description of the experimental data. As in the original data analysis [39], for the WS wave functions the radius of the potential was chosen to reproduce the width of the experimental distribution. On the other hand, no free parameters are used in the nonrelativistic HF and in the relativistic Dirac-Hartree wave functions, that are able to give an equivalently good description of data.

In order to reproduce the magnitude of the experimental data, a reduction factor has been applied in Fig. 1 to all the theoretical results. These factors, listed in Tab. III, have been determined by a fit of the calculated reduced cross sections to the data over the whole missing-momentum range considered in the experiment. The reduction factors applied to the DWIA-WS results are identical to those obtained in the data analysis of Ref. [39], where the same optical potential and WS wave functions were used.

In RDWIA calculations the $cc2$ expression for the current operator [63] has been used. Different expressions can give an equivalently good agreement with the shape of the experimental momentum distribution, but somewhat different reduction factors must be applied to reproduce the magnitude of the experimental reduced cross sections [15, 27]. We

checked that the reduction factors are about 10% smaller when the *cc*1 current is used, and about 10% larger with the *cc*3 current.

In all the calculations the reduction factors obtained for the transition to the $3/2^+$ ground state in perpendicular kinematics are about 20-25% lower than those obtained in parallel kinematics. The source of this difference is not clear. It may have an experimental motivation, or it may be due to effects that give different contributions in different kinematics and that are not adequately considered in the model. In any case, the difference reflects the uncertainties in the identification of the spectroscopic factor as a simple reduction factor of the theoretical results with respect to the experimental data.

Measurements for the ^{48}Ca $(e, e'p)$ reaction were carried out at NIKHEF in parallel kinematics [39]. Thus, for calcium isotopes, we have the opportunity to test the evolution of our theoretical input against the change of neutron number in comparison with the experimental data. The comparison between our DWIA and RDWIA results and the ^{48}Ca $(e, e'p)$ data is shown in Fig. 2 for the transitions to the $1/2^+$ ground state and to the first $3/2^+$ excited state at $E_x = 0.36$ MeV of ^{47}K.

As in the case of ^{40}Ca, all the theoretical results give a very good description of the shape of the experimental momentum distribution. Also in this case, reduction factors have been applied to all the calculated reduced cross sections presented in the figure. These factors are listed in Tab. III. For the DWIA-WS results the reduction factors are identical to those obtained in the data analysis of Ref. [40]. We notice that for all our model calculations the reduction factors obtained for the $1d_{3/2}$ state of ^{48}Ca are consistently lower than those obtained for the $1d_{3/2}$ state of ^{40}Ca in the same parallel kinematics.

In Fig. 3 we compare our results with the ^{16}O $(e, e'p)$ data measured at NIKHEF in parallel kinematics [41] for the transition to the $1/2^-$ ground state of ^{15}N, which is obtained by knocking out a proton from the $1p_{1/2}$ s.p. level. Also in this case, the results of our calculations are multiplied by the reduction factors given in Tab. III. The DWIA-WS reduced cross section gives a good description of the data. As in the calcium cases, the value of the reduction factor is the same obtained in the data analysis of Ref. [41], where the same bound-state wave function and optical potential were used.

Also the RDWIA calculation gives a good description of the data. This is the same result presented in [23], and also the same reduction factor has been applied. The situation is slightly different for the DWIA result obtained with the HF wave function. In this case, the description of the shape of the experimental momentum distribution is slightly worse. We observe that the width of the HF distribution is larger than that shown by the data and well reproduced by the other calculations. This indicates that the rms radius of the $1p_{1/2}$ HF wave function is smaller than those of the WS and relativistic wave functions (see Tab. I). We observe in Tab. III that the reduction factor 0.89, that has been applied to the DWIA-HF result to reproduce the magnitude of the experimental data in the maximum region, is remarkably larger than those applied to the DWIA-WS and RDWIA results. We notice that this large value has been obtained fitting the maximum of the experimental reduced cross section, and not through a best fit to the whole momentum distribution like with DWIA-WS and RDWIA. Moreover, a poor description of the experimental shape does not permit a reliable determination of the spectroscopic factor.

Our nuclear models have been used to calculate $(e, e'p)$ cross sections for other oxygen and calcium isotopes. We intend to investigate how the characteristics of the s.p. proton wave functions, describing the initial hole state, evolve as a function of the neutron number and how this evolution affects the $(e, e'p)$ cross sections.

Once the effective interaction is chosen, the HF and the relativistic Dirac-Hartree approaches are parameter-free, and automatically provide s.p. energies and wave functions for each nucleus. The situation is different in the phenomenological approach, where the parameters of the WS wells change for each nucleus. We changed the radius of the well by using the empirical $R = r_o A^{1/3}$ rule. Moreover, the depths of the wells are determined to obtain the experimental separation energies taken from the compilation of Refs. [64–66].

We first discuss the results obtained for the calcium isotopes. We have considered the ^{40,48,52,60}Ca isotopes, since they are spherical nuclei where the s.p. levels are fully occupied and the pairing effects are negligible. For all these isotopes we have considered proton knock-out emission from the $1d_{3/2}$ and $2s_{1/2}$ states. Our results are shown in Fig. 4 for parallel kinematics and in Fig. 5 for $(\boldsymbol{q}, \omega)$ constant kinematics. The values of all the kinematic variables are the same as in Figs. 1 and 2. The only difference is that, since the separation energy of the proton increases with increasing number of neutrons, we changed, for the different isotopes, the energy of the outgoing electron, and consequently the energy transfer, in order to keep constant, via energy conservation, the energy of the outgoing proton. We have verified that these differences in the kinematic variables do not produce significant effects on the final results.

In Figs. 4 and 5 we compare the reduced cross sections calculated for the various isotopes obtained by using the three different nuclear models: DWIA-WS, DWIA-HF, and RDWIA. The comparison illustrates how these models describe the effects produced by the asymmetry between the number of neutrons and protons. No reduction factors have been applied to the curves presented in these figures.

It is interesting to remark that the evolution of the cross section with respect to the change of the neutron number is the same in all the panels of both figures. We observe that the ^{40}Ca lines are always above the other ones, and

the size of the curves decreases with the increasing number of neutrons. This behavior is clearer in the DWIA-WS results, panels (a) and (b) of both figures, and becomes less evident in the other cases, especially in the RDWIA ones.

For a better understanding of these results it is interesting to consider the s.p. hole wave functions obtained in the three models. We show in Fig. 6 the squared moduli of the radial part of the s.p wave function for the $1d_{3/2}$ and $2s_{1/2}$ states of the various calcium isotopes. The relativistic wave functions shown in the figure are obtained by summing the squared of the radial part of the upper and lower components of the Dirac spinor. All the curves shown in the figure are normalized to one.

The behavior of the WS wave functions shown in panels (a) and (b) can be understood by considering that the depth of the WS well becomes deeper with increasing neutron number. This deepening occurs because by increasing the neutron number the proton experiences more binding, its separation energy increases, and the depth of the WS well, which is determined to reproduce the experimental separation energy, increases. A deeper WS well produces narrower wave functions, as the curves of the upper panels of Fig. 6 show.

The HF wave functions have a different behavior, as shown in panels (c) and (d). In this case, the narrower wave functions are those obtained for the isotopes with smaller neutron numbers. The behavior of the relativistic wave functions is somewhat different and does not have a defined trend as in the previous cases. It is, in any case, more similar to that of the HF than to that of the WS wave functions. We point out that the values of the separation energies, and their trend as a function of the neutron number, are similar in all three types of calculation.

These differences in the wave functions are responsible for only a part of the differences in the reduced cross sections of Figs. 4 and 5, which show a different trend as a function of neutron number. While in the PWIA the reduced cross section contains only information on the bound-state wave function, in the DWIA this information is modified by the contribution of the other ingredients of the model, such as FSI and the electron-nucleon interaction. All these contributions are intertwined in the calculated cross section and, in general, they cannot be easily disentangled.

In order to understand the source of the difference between the behavior of the wave functions and of the cross sections with respect to the increase of neutron number, we have performed PWIA calculations. In this case, FSI are switched off and the $(e, e'p)$ cross section is directly proportional to the squared modulus of the Fourier transform of the hole s.p. wave function. We have checked that the trend of our PWIA results agrees with the trend of the wave functions shown in Fig. 6: the WS wave functions produce PWIA reduced cross sections higher for ^{40}Ca than for the other nuclei, while the situation is reversed with the HF wave functions. As a next step, we have done DWIA calculations by using the same parameters of the optical potential for all the isotopes. The results are different from those obtained in the PWIA, but the trends, with respect to the change of the neutron number, are preserved. Only when we include that A-dependence of the optical potential are the trends of the cross sections changed and also the DWIA-HF results produce ^{40}Ca $(e, e'p)$ reduced cross sections larger than those obtained for the other isotopes.

The dependence of the wave functions on the proton to neutron asymmetry is responsible for a large part of the differences in the reduced cross sections, but an important and crucial contribution is given by FSI, which are described in the calculations by phenomenological optical potentials. The differences between the results in parallel and $(\boldsymbol{q}, \omega)$ constant kinematics in Figs. 4 and 5 are basically due to the different effects of the distortion produced by the optical potential. These effects strongly depend on kinematics and are larger in parallel than in $(\boldsymbol{q}, \omega)$ constant kinematics [2, 3, 5].

The s.p. bound states adopted in the present calculations are normalized to unity and no reduction factor has been applied to the results shown in Figs. 4 and 5 . The comparison with data in Figs. 1 and 2 gives, however, a significant quenching of the measured cross sections with respect to the predictions of the MF model. The quenching is different for the ^{40}Ca $(e, e'p)$ and ^{48}Ca $(e, e'p)$ reactions and increases with neutron number. A quenching depending on the number of neutrons can be expected for all the isotopes and would give further differences on the reduced cross sections than those shown in Figs. 4 and 5.

The behavior of the $(e, e'p)$ cross sections on nuclei with increasing neutron number that we have just presented is not specific to the calcium isotopes. An analogous behavior is found also for the oxygen isotopes. In our calculations we have considered the ^{16,22,24,28}O nuclei. We show in Fig. 7 the reduced cross sections of the $(e, e'p)$ reaction, calculated for the emission of a $1p_{1/2}$ proton in these nuclei by using our three models. The calculations have been done in the same parallel kinematics as in Fig. 3, and we included the small differences due to the different proton separation energies of the different isotopes, as explained in the case of the calcium isotopes.

The radial s.p wave functions squared are plotted in Fig. 8. Also in this case, the different behavior of the WS and HF radial wave functions with respect to the change in neutron number is evident. This difference is not present in the results of Fig. 3. We have repeated also for the oxygen isotopes the investigation done for the calcium isotopes by doing PWIA calculations and DWIA calculations with the same optical potential for all the isotopes. We obtained results analogous to those discussed for the calcium isotopes.

IV. SUMMARY AND CONCLUSIONS

In this work we have presented and discussed $(e, e'p)$ cross sections calculated for a set of calcium and oxygen isotopes with the aim of studying their evolution with respect to the change of neutron number. The calcium and oxygen isotopes have been chosen since data are available for the doubly magic ^{40}Ca, ^{48}Ca, and ^{16}O nuclei. In the calcium and oxygen isotope chains, we have considered only those nuclei with fully occupied s.p. levels, since they are spherical and, moreover, pairing effects are negligible.

The general framework that we have considered for the description of the $(e, e'p)$ process is based on the one-nucleon knock out picture [3, 42] and it is well established. The nonrelativistic DWIA and relativistic RDWIA models used for the calculations were widely and successfully applied to the analysis of the available $(e, e'p)$ data over a wide range of stable nuclei. The results obtained with three different descriptions of the hole wave function of the knocked out proton, all of them based on the mean field approximation, have been compared. We have performed DWIA calculations with phenomenological WS and HF wave functions. For ^{16}O, ^{40}Ca, and ^{48}Ca nuclei the WS wave functions are the same as used in the original analyses of the experimental data in [39–41]. The wave functions used in the RDWIA are obtained by solving Dirac-Hartree equations.

The three models are all able to give a good and similar description of the shape of the experimental reduced cross section on ^{16}O,^{40}Ca, and ^{48}Ca target nuclei, with the only exception of the HF result in ^{16}O. In order to reproduce the magnitude of the experimental data, a reduction factor has been applied to all the calculated results.

In our study of the $(e, e'p)$ process in the two isotope chains we have found that the general behavior of the cross sections with respect to the increasing number of neutrons is analogous for all the three models. Generally speaking, the reduced cross sections are larger and narrower for the lighter isotopes, and evolve by lowering and widening with increasing neutron number.

The behavior of the hole s.p. wave functions for the three models show rather different trends: the WS wave functions become narrower and have higher maxima with increasing neutron number, the HF wave functions show an opposite behavior, and the behavior of the relativistic wave functions is not so well defined, but it is more similar to the behavior of HF than of the WS wave functions.

The dependence of the wave functions on the proton to neutron asymmetry is responsible for only a part of the differences in the reduced cross sections. An important and crucial contribution is also given by FSI, that are described in the calculations by phenomenological optical potentials. The optical potential is an important ingredient of the model that affects both the size and the shape of the cross section in a way that strongly depends on kinematics. In particular, its imaginary part, that gives a reduction of the nucleon flux and, consequently, of the calculated cross section, can affect the values of the spectroscopic factors obtained from the comparison between data and theoretical results. In the present calculations we have used phenomenological optical potentials that were usually adopted in the previous DWIA and RDWIA analyses of $(e, e'p)$ data on stable closed-shell nuclei. The dependence of the optical potential on the asymmetry between the number of neutrons and protons is an interesting problem that deserves careful investigation.

We have used MF wave functions that do not include correlations. The reduction factors found in comparison with the experimental data can provide a measure of the effects not included in the calculations and, under certain conditions, can be identified with the spectroscopic factors. In the comparison of our $(e, e'p)$ cross sections calculated for the various calcium and oxygen isotopes, and shown in Figs. 4, 5, and 7, we did not apply reduction factors, since data are available only for the ^{16}O, ^{40}Ca, and ^{48}Ca target nuclei.

From recent experimental and theoretical studies there are indications that the spectroscopic factors and the effects of correlations depend on the asymmetry between the number of neutrons and protons. Recent experimental information on the spectroscopic factors of drip-line isotopes has been obtained by means of nucleon knockout using intermediate heavy-ion beams [67–69]. These results also include neutron data and suggest a strong dependence of the spectroscopic factors on the proton-neutron ratio. In general, the quenching of quasiparticle orbits, and hence correlations, becomes stronger with increasing separation energy.

From the theoretical point of view, a dependence on nucleon asymmetry has been found in [70] for the depletion of the Fermi sea in asymmetric nuclear matter, with the minority nucleonic species becoming more depleted, and the majority one less. Results of Faddeev-random=phase approximation calculations for the spectroscopic factors of $^{16-28}$O and $^{40-60}$Ca isotopes [71] show that the spectroscopic factors become smaller with increasing nucleon separation energy. From recent work on the dispersive optical potential, which has been applied to calcium isotopes with the aim to extract the asymmetry dependence of the self-energy, a clear signal emerges suggesting that the surface imaginary term of the dispersive optical potential increases with the asymmetry for protons [72–74]. Apart from the associated increased binding that protons experience with increasing asymmetry, there is a corresponding reduction of valence hole spectroscopic factors.

Therefore, we can expect a dependence of the spectroscopic factors on the neutron number and this would give further differences in the reduced cross sections than those shown in Figs. 4, 5, and 7.

Measurements of the exclusive quasifree $(e, e'p)$ cross section on nuclei with neutron excess would offer a unique opportunity for studying the dependence of the properties of bound protons and of nucleon-nucleon correlations on the neutron to proton asymmetry. In this work models that have proven their reliability in the comparison with $(e, e'p)$ data on stable nuclei have been used to investigate the evolution of the $(e, e'p)$ cross sections with increasing proton-neutron asymmetry. Although the models and the theoretical ingredients adopted in the calculations contain approximations, our results can serve as a useful first reference for possible future experiments. The comparison with data can confirm or invalidate the predictions of our models and test the ability of the established nuclear theory in the domain of exotic nuclei.

[1] S. Frullani, J. Mougey, Adv. Nucl. Phys 14 (1984) 1.
[2] S. Boffi, C. Giusti, F. D. Pacati, Phys. Rep. A 226 (1993) 1.
[3] S. Boffi, C. Giusti, F. Pacati, M. Radici, Electromagnetic response of atomic nuclei, Clarendon, Oxford, 1996.
[4] J. Mougey, et al., Nucl. Phys. A 262 (1976) 461.
[5] M. Bernheim, et al., Nucl. Phys. A 375 (1982) 381.
[6] P. K. A. de Witt Huberts, J. Phys. G 16 (1990) 507.
[7] L. Lapikás, Nucl. Phys. A 553 (1993) 297c.
[8] K. I. Blomqvist, et al., Phys. Lett. B 344 (1995) 85.
[9] C. Giusti, F. D. Pacati, Nucl. Phys. A 473 (1987) 717.
[10] C. Giusti, F. D. Pacati, Nucl. Phys. A 485 (1988) 461.
[11] A. Picklesimer, J. W. V. Orden, S. J. Wallace, Phys. Rev. C 32 (1985) 1312.
[12] Y. Jin, D. S. Onley, L. E. Wright, Phys. Rev. C 45 (1992) 1311.
[13] Y. Jin, J. K. Zhang, D. S. Onley, L. E. Wright, Phys. Rev. C 47 (1993) 2024.
[14] Y. Jin, D. S. Onley, Phys. Rev. C 50 (1994) 377.
[15] J. M. Udías, P. Sarriguren, E. M. de Guerra, E. Garrido, J. A. Caballero, Phys. Rev. C 48 (1993) 2731.
[16] J. M. Udías, P. Sarriguren, E. M. de Guerra, J. A. Caballero, Phys. Rev. C 53 (1996) R1488.
[17] J. M. Udías, J. A. Caballero, E. M. de Guerra, J. E. Amaro, T. W. Donnelly, Phys. Rev. Lett. 83 (1999) 5451.
[18] J. J. Kelly, Phys. Rev. C 56 (1997) 2672.
[19] J. J. Kelly, Phys. Rev. C 59 (1999) 3256.
[20] J. J. Kelly, Phys. Rev. C 60 (1999) 044609.
[21] M. Hedayati-Poor, J. I. Johansson, H. S. Sherif, Phys. Rev. C 51 (1995) 2044.
[22] J. I. Johansson, H. S. Sherif, G. M. Lotz, Nucl. Phys. A 605 (1996) 517.
[23] A. Meucci, C. Giusti, F. D. Pacati, Phys. Rev. C 64 (2001) 014604.
[24] A. Meucci, C. Giusti, F. D. Pacati, Phys. Rev. C 64 (2001) 064615.
[25] A. Meucci, Phys. Rev. C 65 (2002) 044601.
[26] A. Meucci, C. Giusti, F. D. Pacati, Phys. Rev. C 66 (2002) 034610.
[27] M. Radici, A. Meucci, W. H. Dickhoff, Eur. Phys. Jou. A 17 (2003) 65.
[28] T. Tamae, et al., Phys. Rev. C 80 (2009) 064601.
[29] J. Gao, et al., Phys. Rev. Lett. 84 (2000) 3265.
[30] S. Malov, et al., Phys. Rev. C 62 (2000) 057302.
[31] I. Tanhihata, Prog. Part. Nucl. Phys. 35 (1995) 505.
[32] H. Geissel, G. Müzenberg, R. Riisager, Annu. Rev. Nucl. Part. Sci. 45 (1995) 163.
[33] A. Mueller, Prog. Part. Nucl. Phys. 46 (2001) 359.
[34] T. Suda, K. Maruyama, I. Tanhihata, RIKEN Accel. Prog. Rep. 34 (2001) 49.
[35] T. Katayama, T. Suda, I. Tanhihata, Physica Scripta T104 (2003) 129.
[36] An International Accelerator Facility for Beams of Ions and Antiprotons, GSI report 2006 `http://www.gsi.de/GSI-Future/cdr/` (2006).
[37] `http://www.gsi.de/forschung/fair_experiments/elise/index_e.html`.
[38] T. Suda, A construction proposal of an electron scattering facility for structure studies of short-lived nuclei, Proposal for Nuclear Physics Experiments at RIBF NP1006 – SCRIT01 (2010).
[39] G. J. Kramer, The proton spectral function of ^{40}Ca and ^{48}Ca studied with the (e,e′p) reaction, Ph.D. thesis, Universiteit Amsterdam (Nederlands), unpublished (1990).
[40] G. J. Kramer, H. P. Blok, L. Lapikás, Nucl. Phys. A 679 (2001) 267.
[41] M. Leuschner, et al., Phys. Rev. C 49 (1994) 955.
[42] S. Boffi, F. Cannata, F. Capuzzi, C. Giusti, F. D. Pacati, Nucl. Phys. A 379 (1982) 509.
[43] A. N. Antonov, P. E. Hodgson, I. Z. Petkov, Nucleon momentum and density distributions, Clarendon, Oxford, 1988.
[44] A. N. Antonov, P. E. Hodgson, I. Z. Petkov, Nucleon Correlations in Nuclei, Springer-Verlag, Berlin, 1993.
[45] W. H. Dickhoff, C. Barbieri, Prog. Part. Nucl. Phys. 52 (2004) 377.
[46] P. Schwandt, H. O. Meyer, W. W. Jacobs, A. D. Bacher, S. E. Vigdor, M. D. Kaitchuck, T. R. Donoghue, Phys. Rev. C 26 (1982) 55.
[47] M. Hedayati-Poor, J. I. Johansson, H. S. Sherif, Nucl. Phys. A 593 (1995) 377.
[48] E. D. Cooper, S. Hama, B. C. Clark, R. L. Mercer, Phys. Rev. C 47 (1993) 297.
[49] M. K. Gaidarov, K. A. Pavlova, A. N. Antonov, M. V. Stoitsov, S. S. Dimitrova, M. V. Ivanov, C. Giusti, Phys. Rev. C 61 (2000) 014306.
[50] M. V. Ivanov, M. K. Gaidarov, A. N. Antonov, C. Giusti, Phys. Rev. C 64 (2001) 014605.
[51] H. Müther, A. Polls, W. H. Dickhoff, Phys. Rev. C 51 (1995) 3040.
[52] D. V. Neck, M. Waroquier, A. E. L. Dieperink, S. C. Pieper, V. R. Pandharipande, Phys. Rev. C 57 (1998) 2308.
[53] D. Rohe, et. al., Phys. Rev. Lett. 93 (2004) 182501.
[54] R. Subedi, et al., Science 320 (2008) 1476.
[55] C. Barbieri, Phys. Rev. Lett. 103 (2009) 202502.
[56] G. Co', A. M. Lallena, Nuov. Cim. A 111 (1998) 527.

[57] A. R. Bautista, G. Co', A. M. Lallena, Nuov. Cim. A 112 (1999) 1117.
[58] J. F. Berger, M. Girod, D. Gogny, Comp. Phys. Commun. 63 (1991) 365.
[59] S. Goriely, S. Hilaire, M. Girod, S. Péru, Phys. Rev. Lett. 102 (2009) 242501.
[60] C. J.Horowitz, B. D.Serot, Phys. Lett. B 86 (1979) 146.
[61] C. J.Horowitz, B. D.Serot, Nucl. Phys. A 368 (1981) 503.
[62] C. J. Horowitz, D. P. Murdoch, B. D. Serot, Computational Nuclear Physics I: Nuclear Structure, Springer-Verlag, Berlin, 1991.
[63] T. de Forest, Jr., Nucl. Phys. A 392 (1983) 232.
[64] G. Audi, A. H. Wapstra, C. Thibault, Nucl. Phys. A 729 (2003) 337.
[65] `http://ie.lbl.gov/toi2003/MassSearch.asp`.
[66] `http://www.nndc.bnl.gov`.
[67] P. G. Hansen, J. A. Tostevin, Ann. Rev. Nucl Part. Sci. 53 (2003) 219.
[68] A. Gade, et al., Phys. Rev. Lett. 93 (2004) 042501.
[69] A. Gade, et al., Phys. Rev. C 77 (2008) 044306.
[70] A. Rios, A. Polls, W. H. Dickhoff, Phys. Rev. C 79 (2009) 064308.
[71] C. Barbieri, W. H. Dickhoff, Int. J. Mod. Phys. A 24 (2009) 2060.
[72] R. J. Charity, L. G. S. Hama, W. H. Dickhoff, Phys. Rev. Lett. 97 (2006) 162503.
[73] R. J. Charity, J. M. Mueller, L. G. S. Hama, W. H. Dickhoff, Phys. Rev. C 76 (2007) 044314.
[74] W. H. Dickhoff, J. Phys. G: Nucl. Part. Phys. 37 (2010) 064007.

nucleus		S_p [MeV] $1p_{1/2}$	r_{rms} [fm] $1p_{1/2}$	r^P_{rms} [fm]	r^N_{rms} [fm]
^{16}O	WS	-12.127	2.94		
	HF	-11.906	2.83	2.63	2.61
	REL	-12.294	2.97	2.63	2.60
^{22}O	WS	-23.26	2.77		
	HF	-23.60	2.83	2.68	2.97
	REL	-23.59	2.76	2.59	3.01
^{24}O	WS	-26.60	2.77		
	HF	-25.60	2.89	2.70	3.12
	REL	-23.97	2.83	2.62	3.28
^{28}O	WS	-31.04	2.80		
	HF	-31.04	2.96	2.82	3.42
	REL	-28.65	2.95	2.69	3.58

Table I: Proton separation energies (S_p), rms radii of the $1p_{1/2}$ bound state wave functions (r_{rms}) and of the global proton (r^P_{rms}) and neutron (r^N_{rms}) density distributions, obtained with the different MF models for all the oxygen isotopes we have considered.

nucleus		S_p [MeV] $1d_{3/2}$	r_{rms} [fm] $1d_{3/2}$	S_p [MeV] $2s_{1/2}$	r_{rms} [fm] $2s_{1/2}$	r^P_{rms} [fm]	r^N_{rms} [fm]
^{40}Ca	WS	-8.328	3.69	-10.85	3.72		
	HF	-8.753	3.58	-9.92	3.59	3.37	3.33
	REL	-8.704	3.73	-9.20	3.87	3.38	3.33
^{48}Ca	WS	-15.907	3.54	-15.807	3.58		
	HF	-16.542	3.63	-16.18	3.55	3.41	3.55
	REL	-15.606	3.60	-13.815	3.64	3.37	3.59
^{52}Ca	WS	-17.80	3.54	-20.0	3.58		
	HF	-18.83	3.67	-19.98	3.55	3.46	3.70
	REL	-16.75	3.68	-16.494	3.72	3.41	3.85
^{60}Ca	WS	-25.200	3.53	-24.96	3.53		
	HF	-25.200	3.83	-24.96	3.64	3.59	3.98
	REL	-20.744	3.75	-20.288	3.76	3.51	4.15

Table II: The same as in Tab. I for the $1d_{3/2}$ and $2s_{1/2}$ proton states for all the calcium isotopes we have considered.

		DWIA-WS	DWIA-HF	RDWIA	
$(3/2^+;\ ^{39}\mathrm{K})$	$\parallel$	0.65	0.64	0.69	Fig. 1
$(3/2^+;\ ^{39}\mathrm{K})$	$\perp$	0.49	0.51	0.49	Fig. 1
$(1/2^+;\ ^{39}\mathrm{K})$	$\parallel$	0.52	0.57	0.51	Fig. 1
$(1/2^+;\ ^{39}\mathrm{K})$	$\perp$	0.55	0.62	0.51	Fig. 1
$(3/2^+;\ ^{47}\mathrm{K})$	$\parallel$	0.56	0.55	0.52	Fig. 2
$(1/2^+;\ ^{47}\mathrm{K})$	$\parallel$	0.54	0.58	0.55	Fig. 2
$(1/2^-;\ ^{15}\mathrm{N})$	$\parallel$	0.64	0.89	0.70	Fig. 3

Table III: Reduction factors applied to the calculated reduced cross sections. We have indicated the spin and parity of the state of the residual nucleus. The symbols $\parallel$ and $\perp$ indicate the parallel and perpendicular or $(\boldsymbol{q}, \omega)$ constant kinematics, respectively.

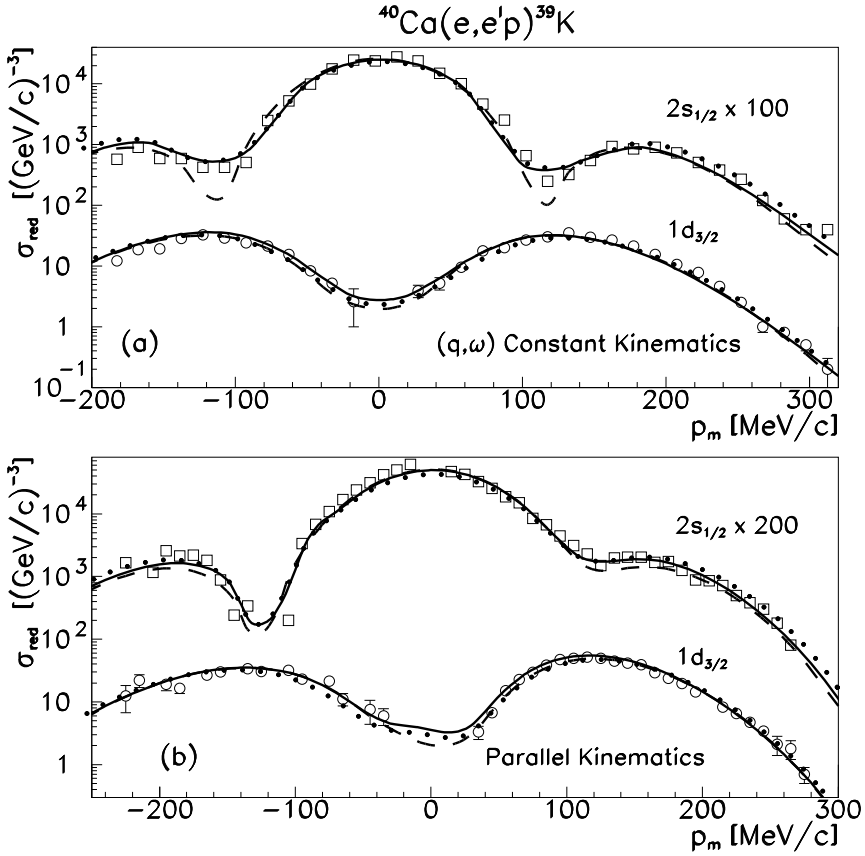

Figure 1: Reduced cross sections of the ^{40}Ca $(e, e'p)$ reaction as a function of the missing momentum $p_{\rm m}$ for the transitions to the $3/2^+$ ground state and to the $1/2^+$ excited state at 2.522 MeV of ^{39}K. In panel (a) we show the results obtained in $(\boldsymbol{q}, \omega)$ constant kinematics, with incident electron energy $E_0 = 483.2$ MeV, electron scattering angle $\vartheta = 61.52^\circ$, and $q = 450$ MeV/c. In panel (b) we show the results obtained in parallel kinematics, with $E_0 = 483.2$ MeV. The outgoing proton energy is $T' = 100$ MeV in both kinematics. The experimental data are taken from Ref. [39]. The solid lines give the DWIA-WS results, the dotted lines the DWIA-HF results, and the dashed lines the RDWIA results. The meaning of the negative values of $p_{\rm m}$ is explained in the text. The theoretical results have been multiplied by the reduction factors presented in Tab. III.

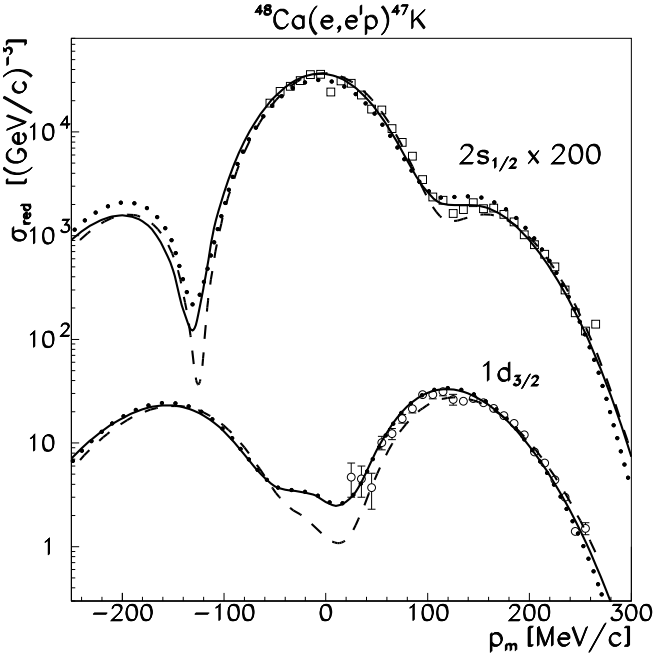

Figure 2: Reduced cross section of the ^{48}Ca $(e, e'p)$ reaction as a function of $p_{\rm m}$ for the transitions to the $1/2^+$ ground state and to the $3/2^+$ excited state at 0.36 MeV of ^{47}K in parallel kinematics, with $E_0 = 440$ MeV and $T' = 100$ MeV. The line convention is the same as in Fig. 1. The experimental data are from Ref. [39]. The values of the reduction factors multiplying the theoretical results are given in Table III.

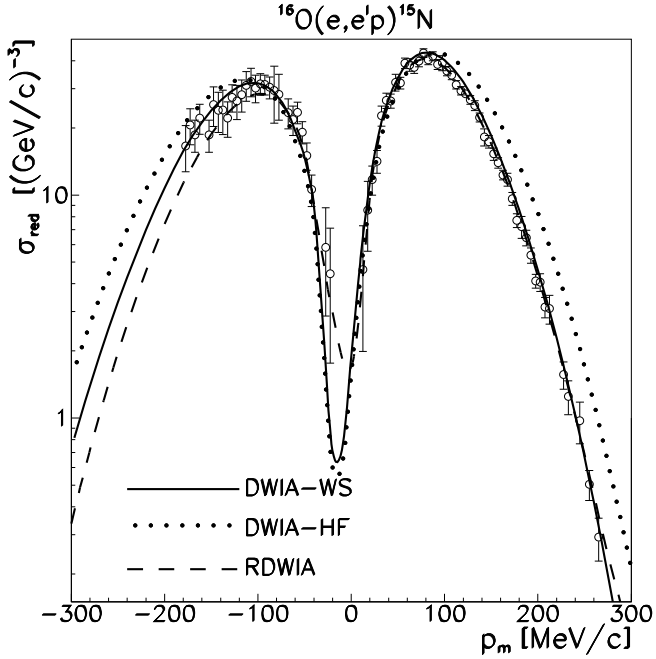

Figure 3: Reduced cross section of the ^{16}O $(e, e'p)$ reaction as a function of $p_{\rm m}$ for the transition to the $1/2^-$ ground state of ^{15}N in parallel kinematics with $E_0 = 520.6$ MeV and $T' = 90$ MeV. The experimental data are from Ref. [41]. The values of the reduction factors multiplying the theoretical results are given in Table III.

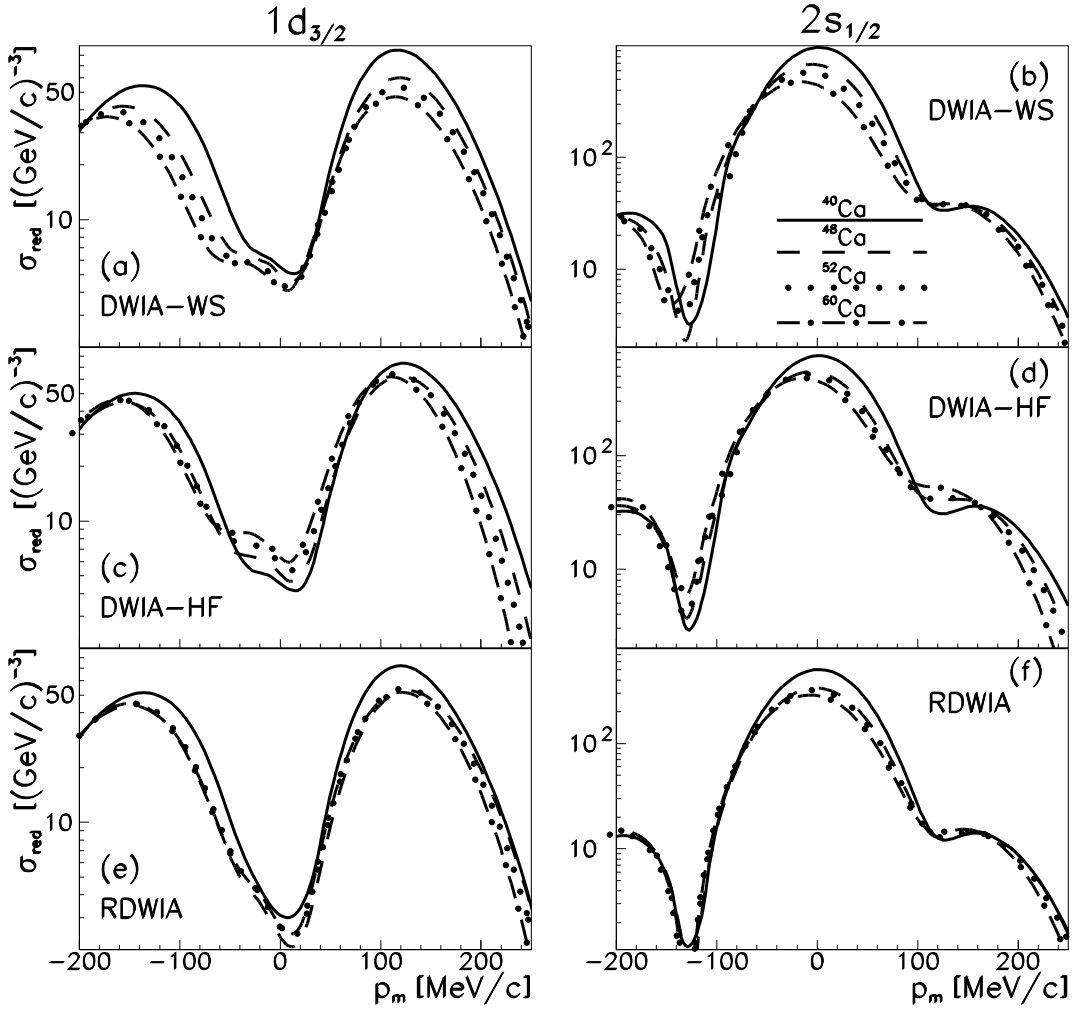

Figure 4: Reduced cross section of the $(e, e'p)$ reaction for $1d_{3/2}$ (left panels) and $2s_{1/2}$ (right panels) knockout from ^{40}Ca (solid lines), ^{48}Ca (dashed lines), ^{52}Ca (dotted lines), and ^{60}Ca (dot-dashed lines), as a function of $p_{\rm m}$. The results of the DWIA-WS calculations are presented in the panels (a) and (b), and those of the DWIA-HF calculations in the panels (c) and (d). The RDWIA results are shown in the panels (e) and (f). The calculations are done in parallel kinematics with $E_0 = 440$ MeV and $T' = 100$ MeV.

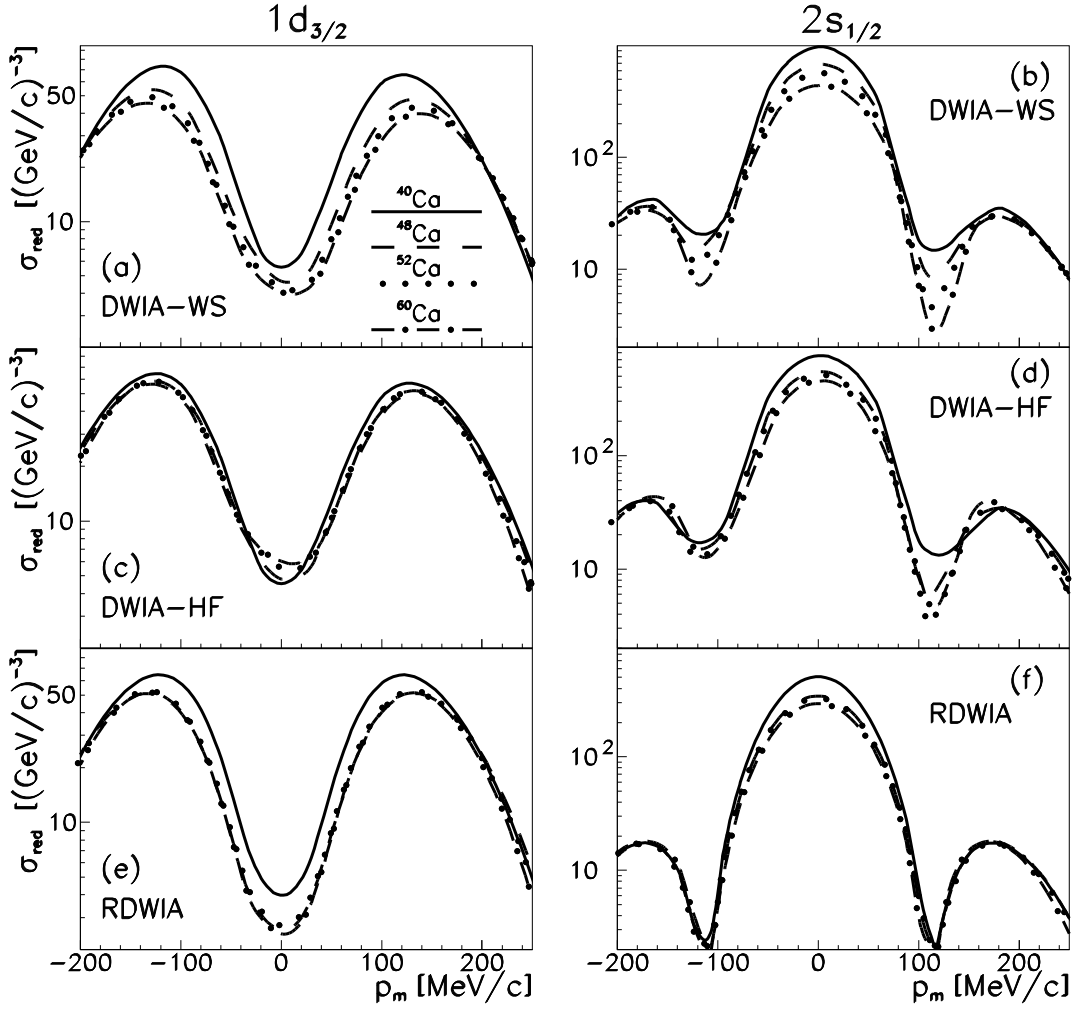

Figure 5: The same as in Fig. 4 but in perpendicular kinematics with $E_0 = 483.2$ MeV, $\vartheta = 61.52^\circ$, and $q = 450$ MeV/c.

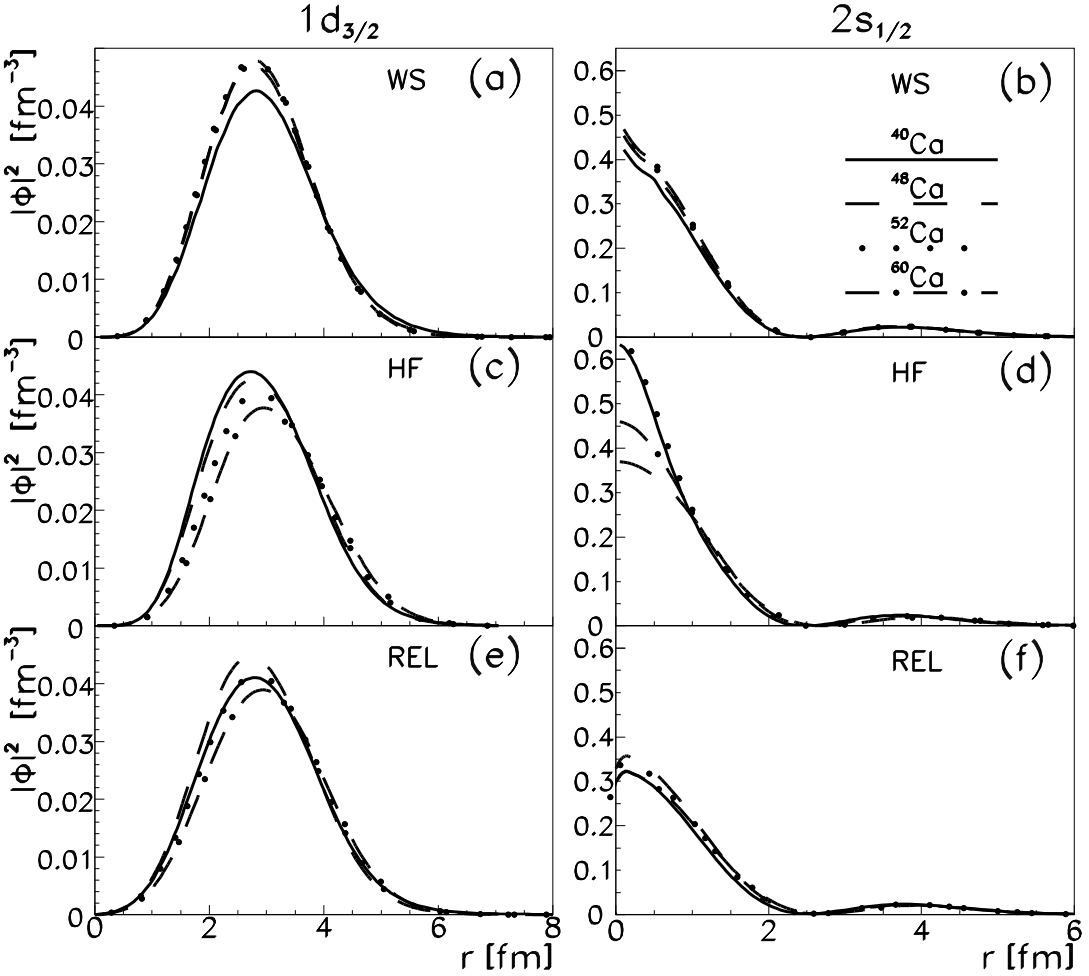

Figure 6: Squared moduli of the radial part of the $1d_{3/2}$ (left panels) and $2s_{1/2}$ (right panels) s.p. wave functions for ^{40}Ca (solid lines), ^{48}Ca (dashed lines), ^{52}Ca (dotted lines), and ^{60}Ca (dot-dashed lines). In panels (a) and (b) we show the WS wave functions, in panels (c) and (d) the HF wave functions, and in panels (e) and (f) the relativistic wave functions obtained in the Dirac-Hartree approach. The normalization of the curves is $\int dr\, r^2\, |\phi|^2 = 1$.

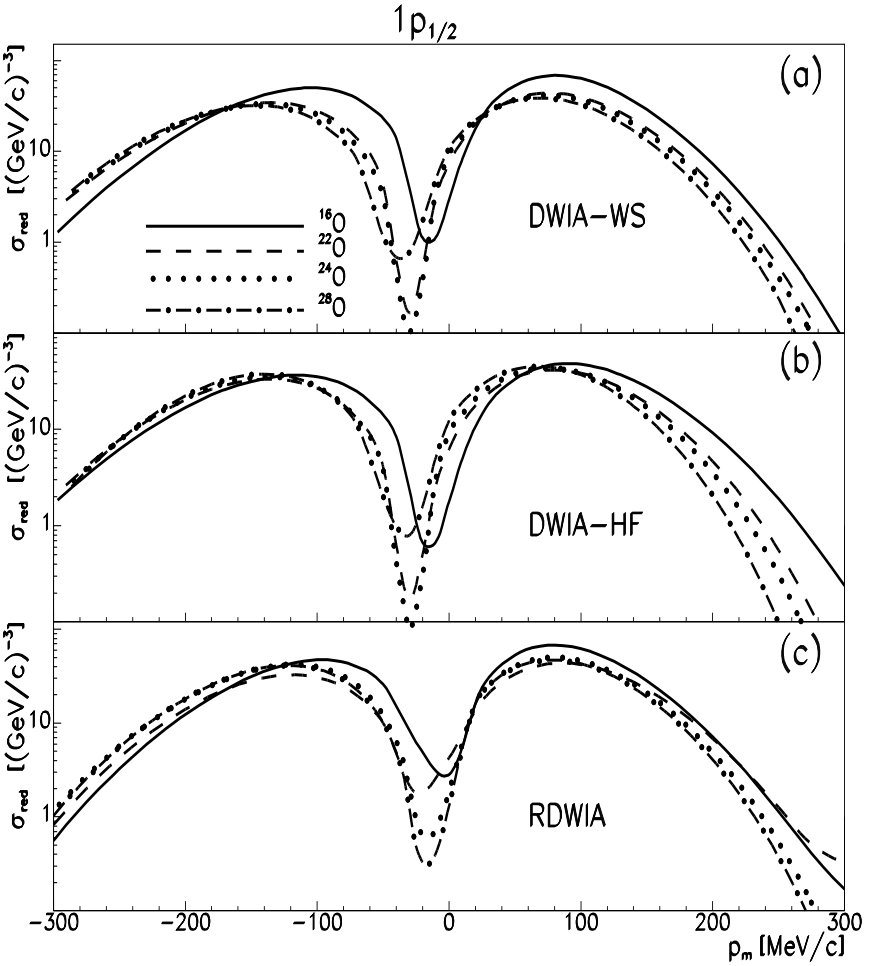

Figure 7: Reduced cross section of the $(e, e'p)$ reaction for $1p_{1/2}$ proton knockout from ^{16}O (solid lines), ^{22}O (dashed lines), ^{24}O (dotted lines), and ^{28}O (dot-dashed lines) as a function of $p_{\rm m}$. In panel (a) we show the DWIA-WS results, in panel (b) the DWIA-HF results, and in panel (c) the RDWIA results. The calculations have been done in parallel kinematics, with $E_0 = 520.6$ MeV and $T' = 90$ MeV.

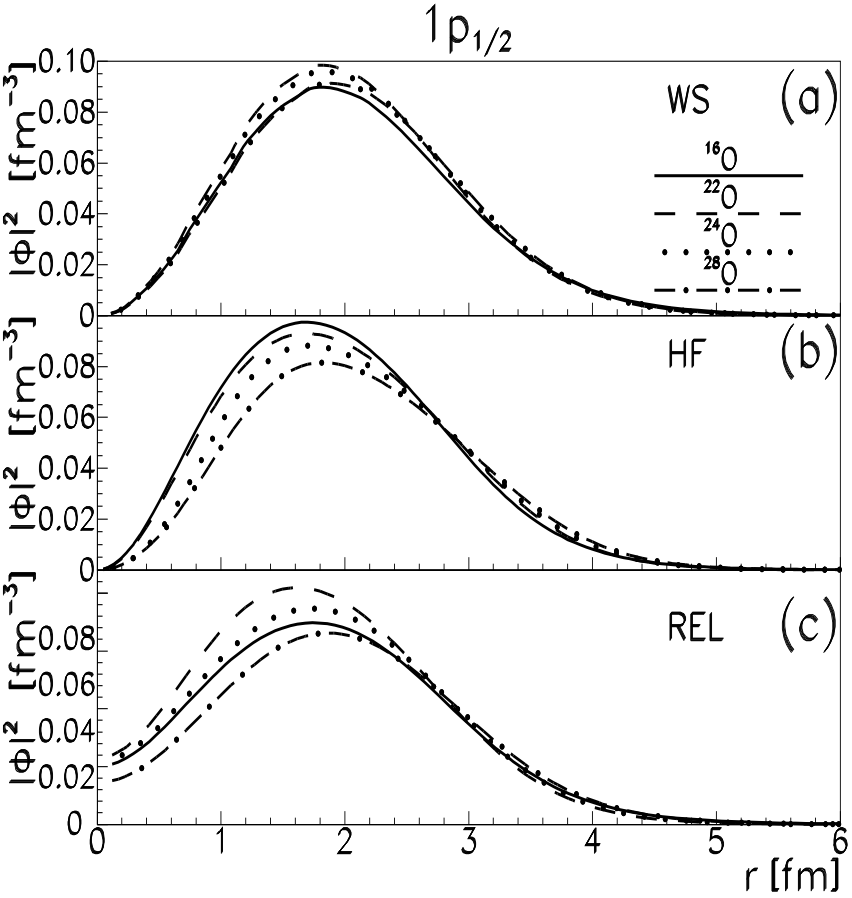

Figure 8: Squared moduli of the radial part of the $1p_{1/2}$ wave functions for ^{16}O (solid lines), ^{22}O (dashed lines), ^{24}O (dotted lines), and ^{28}O (dot-dashed lines). In panel (a) we show the WS wave functions, in panel (b) the HF wave functions, and in panel (c) the relativistic wave functions obtained in the Dirac-Hartree approach. The normalization of the curves is $\int dr\, r^2\, |\phi|^2 = 1$.